

Magnetic Properties of 100 NM-Period Nickel Nanowire Arrays Obtained From Ordered Porous-Alumina Templates

K. Nielsch, R.B. Wehrspohn, S.F. Fischer¹, H. Kronmüller¹, J. Barthel, J. Kirschner, and U. Gösele

Max-Planck-Institute of Microstructure Physics, Weinberg 2, 06120 Halle, Germany

¹Max-Planck-Institute of Metal Research, Heisenbergstr. 1, 70569 Stuttgart, Germany

ABSTRACT

Ni nanowires were grown in highly-ordered anodic alumina templates using pulsed electrodeposition. This technique yields completely metal-filled alumina membranes. The magnetic behavior of 100 nm period arrays of Ni nanowires with a length of 1 μm and different diameters has been characterized using SQUID magnetometry and magnetic force microscopy. Reducing the diameter from initially 50 to 25 nm while keeping the interwire distance constant leads to increasing coercive fields from 600 Oe to 1200 Oe and to increasing remanence from 30% to 100% of the hysteresis. The deposition of $\text{Ni}_{65}\text{Fe}_{35}$ gave a further improvement of the coercive fields up to 1350 Oe.

INTRODUCTION

Magnetic storage plays a key role in the development of information technology. Since 1991, the annual growth rate of the storage density for commercially available hard disks has been 60%. Nowadays, hard disks with an areal density of 10.1 Gbit/in² are commercially available, and a number of companies have demonstrated densities ranging up to 35.5 Gbit/in² in their laboratories. Currently, it takes approximately two years from a laboratory demonstration to the market introduction. If the growth rate for areal densities continues the predicted superparamagnetic limit of about 70 Gbit/in² might be reached in products in a few years [1].

One approach to go beyond this limit is via patterned perpendicular media [2–5], where one bit of information corresponds to one single-domain nanosized particle, a so-called nanomagnet. Since each bit would be composed of a single high-aspect particle, the areal density of this patterned media can, in principle, be more than one order of magnitude higher than in conventional longitudinal media. For example, an areal density of about 300 Gbit/in² can be achieved by a hexagonal arranged array of nanomagnets with a lattice constant of about 50 nm.

One promising technique to obtain nanomagnet arrays is based on hexagonally-arranged porous-alumina templates [6]. We have shown recently that self-ordered porous alumina arrays can be obtained with a sharply defined pore diameter by a two-step electrochemical anodization process of aluminum. The degree of self-ordering is polydomain with a typically domain size of a few microns. Monodomain pore arrays can be obtained by electron-beam lithography [7] or imprint technology [8]. The interpore distance ($D_{\text{INT}} = 50$ to 500 nm), the pore diameter ($0.25 \cdot D_{\text{INT}} < D_{\text{P}} < D_{\text{INT}}$) and the length (200 nm to 200 μm) can be varied over a wide range [7-11].

PREPARATION OF METAL-FILLED POROUS ALUMINA

Hexagonally-ordered porous alumina templates were prepared via a two-step anodization process on a 0.5 mm thick aluminium substrate, which is described in detail in Refs. 7 and 9. Here, we briefly summarize the fabrication process. After the second anodization step, an ordered nanopore array (Fig. 1 a) is obtained with straight pores from top to bottom and a

thickness of typically 1 μm and a pore diameter, D_p , of 25 nm. The parameters are 0.3 M oxalic acid, $U_{ox} = 40$ V and $T = 2^\circ\text{C}$. After the potential has been switched off, the oxalic acid is heated up to 30°C to increase the pore diameter by chemically widening to the required nanomagnet diameter (Fig. 1 b). (Sample A: 3 hr treatment with hot oxalic acid resulting in $D_p \approx 50$ nm; sample B: 1.5 h widening resulting in $D_p \approx 35$ nm and no pore widening for sample C). Next, the barrier layer at the bottom of the pores is thinned by several current anodization steps. Stepwise the applied anodization current is reduced until a barrier layer thickness of the alumina template of less than 10 nm is reached. A detailed description of the pretreatment of the porous alumina structure for the filling process of the pores has been published in Refs. 6, recently.

Using pulsed electrodeposition, we recently succeeded in homogeneously filling these porous alumina templates with nickel using no direct metallic back contact [6]. Nickel was deposited from a highly concentrated Watts-bath-type (300 g/l $\text{NiSO}_4 \cdot 6\text{H}_2\text{O}$, 45 g/l $\text{NiCl}_2 \cdot 6\text{H}_2\text{O}$, 45 g/l H_3BO_3 , pH=4.5, $T=35^\circ\text{C}$) electrolyte on the nearly isolating oxide barrier layer at the pore tips (Fig 1 d) into the pore structure of sample (A), (B) and (C). For the deposition of sample (D) 8 g/l $\text{FeSO}_4 \cdot 7\text{H}_2\text{O}$ was additionally added to the electrolyte. Pulsed electrodeposition was used to improve the homogeneity of the deposition. During a relatively long pulse of negative current [6 ms, $I_{pulse} = -25 \text{ mA/cm}^2$] the metal was deposited on the pore bottom. After the deposition pulse, a short pulse of positive polarization [2 ms, $U_{pulse} = +4\text{V}$] followed to interrupt the electric field at the deposition interface immediately. Next, there was a break of about 1 s to guarantee the diffusion of metal ions to the pore bottom and the removal of deposition by-products from pore tips, so that each pore had a stable pH.

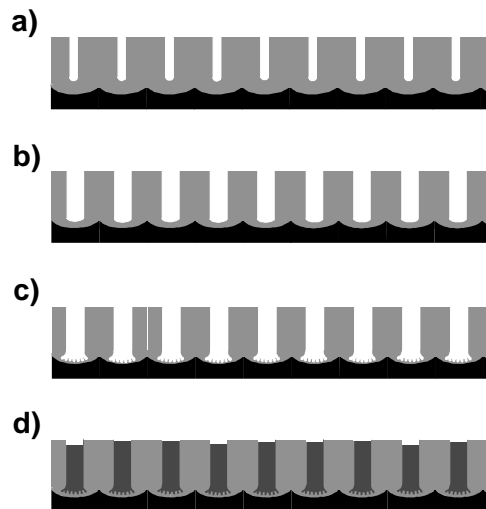


Figure 1: Schematic diagram demonstrating the fabrication of a highly-ordered porous alumina matrix and the preparation steps necessary for the subsequent filling of the structure. A highly-ordered porous alumina template was fabricated by two subsequent anodization steps (a). Pores were widened by isotropic chemical etching (b). To thin the barrier layer further, several current-limited anodization steps followed, with dendrite pores forming at the barrier layer (c). Metal deposition in the pores (d).

To characterize the metal-filled template and its magnetic properties, the top of the template structure was fixed to a silicon substrate by a conducting glue (Fig. 2a). Next, the aluminum substrate was removed by a saturated solution of HgCl and the structure was turned upside down (Fig. 2b). After removing from the top a ≈ 200 nm thick layer of the filled template by a focussed ion beam, which was estimated from the thinning rate, the top ends of the nanowires became visible at the surface and a relatively smooth surface was obtained (Fig. 2c).

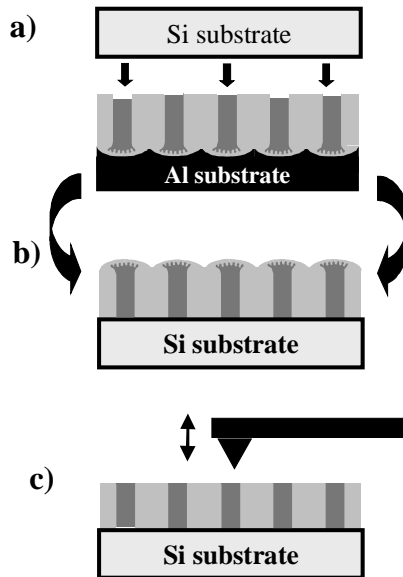


Figure 2: Schematic diagram demonstrating the preparation steps for the subsequent physical characterization of the nickel filled alumina templates. The filled template was attached to a Si substrate (a). The Al substrate was removed by selective chemical etching (b) and the structure was turned upside down. By focussed ion beam milling the barrier layer and dendrite structure were removed and a smooth surface was obtained (c).

Figure 3 shows an SEM image of sample (B). The ferromagnetic nanowires (white) are embedded in the porous alumina matrix (black). Due to the self-organization process, the nanowires are hexagonally arranged with an interwire distance of 100 nm. Sample (B) has a wire diameter of approximately 35 nm. Nearly 100% pore filling was obtained for all three samples discussed, demonstrating that the metallic filling extends over the whole length of the pore [6]. The crystallinity of these samples was further analyzed by X-ray diffraction (XRD). From the θ - 2θ -scan, the average crystallite size is estimated using the Scherrer equation for round particles, yielding an average grain size $D_{Gr} = 10$ to 15 nm.

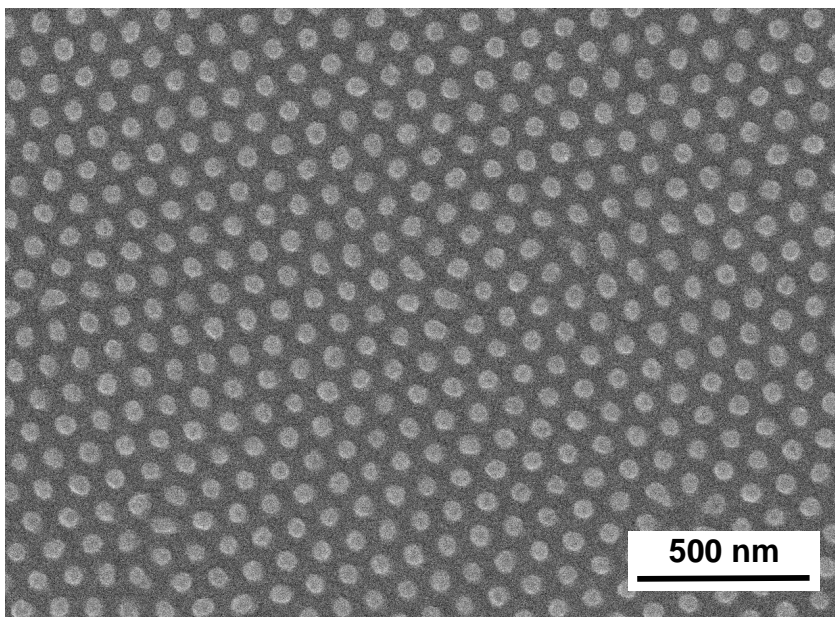


Figure. 3: Top-view SEM micrograph of a nickel-filled alumina membrane with an interpore distance of 100 nm, thinned with ~200 nm removed from the initial surface. The diameter of the Ni columns is $D_p \approx 35$ nm (sample B).

MAGNETIC PROPERTIES AND DISCUSSION

The bulk magnetic properties of metal-filled nanopore arrays were carefully investigated by superconducting quantum interference device magnetometer measurements (SQUID). The field dependent magnetization hysteresis was measured for three nickel-filled samples and one $\text{Ni}_{65}\text{Fe}_{35}$ -filled sample at room temperature. Figure 4 shows the typical bulk magnetization hysteresis loops of hexagonally-ordered Ni nanowire arrays with a pitch of 100 nm, a pore diameter of about $D_P = 50$ nm (sample (A)), 35 nm (sample (B)) and 25 nm (sample (C)). The hysteresis loops measured for these samples with the magnetic field applied parallel to the long axis of the nickel nanowires, shows a coercive field of $H_C^{\parallel} \approx 600$ Oe for $D_P = 50$ nm, $H_C^{\parallel} \approx 1000$ Oe for $D_P = 35$ nm and $H_C^{\parallel} \approx 1200$ Oe for $D_P = 25$ nm. (Fig. 4). The squareness of the hysteresis increases from 30% ($D_P = 50$ nm) up to nearly 100% ($D_P = 25$ nm) with decreasing wire diameter D_P . The measured coercive fields for the hysteresis loops measured perpendicular to the wire are $H_C^{\perp} \approx 150$ Oe and drastically smaller than H_C^{\parallel} . Sample (A) does not show a preferential magnetic orientation, because the saturation fields are similar ($H_S^{\perp} \approx H_S^{\parallel}$) for both measured directions. In contrast, samples (B) and (C) have a preferential magnetic orientation along the wire axis ($H_S^{\parallel} \approx 2000$ Oe, $H_S^{\perp} > 5000$ Oe and $H_C^{\parallel} \gg H_C^{\perp}$).

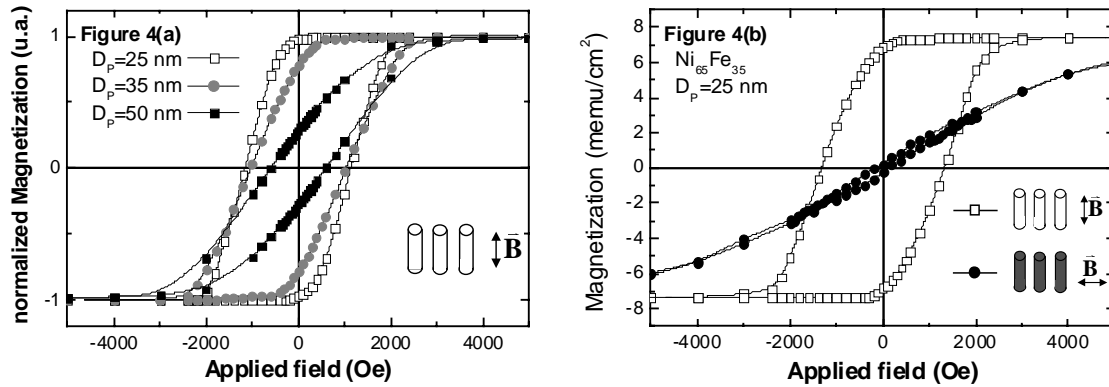


Figure 4 (a): SQUID hysteresis (left) loops for a hexagonally ordered Ni nanowire arrays with a pitch of 100 nm, with a wire length of ≈ 800 nm and a pore diameter of $D_P \approx 50$ nm (sample (A)), ≈ 35 nm (B), and ≈ 25 nm (C) measured with an applied field parallel to the wires. **(b):** Hysteresis loops for a $\text{Ni}_{65}\text{Fe}_{35}$ filled nanowire array with a pitch of 100 nm, column length of ≈ 800 nm and a wire diameter of 25 nm (sample (D)) measured with an applied field parallel and perpendicular to the column axis.

Here, we give only a short description of the analysis of these samples. The detailed analysis of the magnetic properties can be found in Ref. 12. The total magnetic anisotropy of these samples is influenced by the magnetic anisotropy form of the Ni nanowires and the dipole or so-called demagnetization fields between the nanowires. For the same spacing, with decreasing nanowire diameter the dipolar interactions between the nanowires decrease. The switching fields of the individual column increase, so the magnetic hardness and the coercive fields of the hysteresis loops are enhanced. The magneto-crystalline anisotropy of the nanocrystalline Ni wires gives only a small contribution at room temperature. The Ni nanomagnets are single domain particles. Their magnetic reversal process occurs by inhomogeneous switching modes, as confirmed by micromagnetic modeling [13].

The small size distribution of the pore diameter ($\Delta D_P/D_P < 10\%$) [9,11] has a positive impact on the magnetic properties. Here, we report the highest measured coercive fields H_C of about 1200 Oe for a close packed nickel nanowire arrays embedded in a membrane matrix. Previous works on unarranged nickel nanowire arrays show lower coercive fields of about 1000 Oe or less in the preferential magnetic orientation [14,15]. The large size distributions (up to $\Delta D_P/D_P > 50\%$) [16] of the pore diameter and the interwire distance enhance the magnetic interactions in the nanowire arrays and reduce the squareness of the hysteresis.

A further enhancement of the coercive fields was obtained by adding a small amount of iron to the Ni-filling. The hysteresis of a $\text{Ni}_{65}\text{Fe}_{35}$ nanowire array (Fig 4(b): sample (D)) shows a coercive fields of about 1350 Oe and a squareness of about 96% for the direction parallel to the wire axis. It can be seen from both hysteresis loops of sample (D) that the preferential magnetic orientation is parallel to the wire axis. The hysteresis loop for the direction perpendicular to the wire axis shows a small coercive field ($H_C^\perp \approx 100$ Oe) and a high saturation field ($H_S^\perp \approx 8000$ Oe). If we compare the hysteresis loops of sample (C) and (D), which have the same pore diameter, sample (D) has a higher coercivity than sample (C) but a lower squareness. The additional amount of iron in sample (D) leads to an enhancement of the total saturation magnetization M_S of each individual wire. The coercivity and the saturation field increases due to the rise of the theoretical shape effect factor for a nanowire ($2\pi M_S$). Moreover, the interactions between the nanowires increases, due to the enhancement of the average demagnetization field ($-4\pi M_S P$; $P \equiv \text{porosity} \equiv \text{metal filling fraction in the matrix structure}$), which leads to the reduction of the squareness. These investigations suggest that the 25 nm nickel wires are most suitable for patterned perpendicular magnetic media, due the low interaction between the magnetic columns.

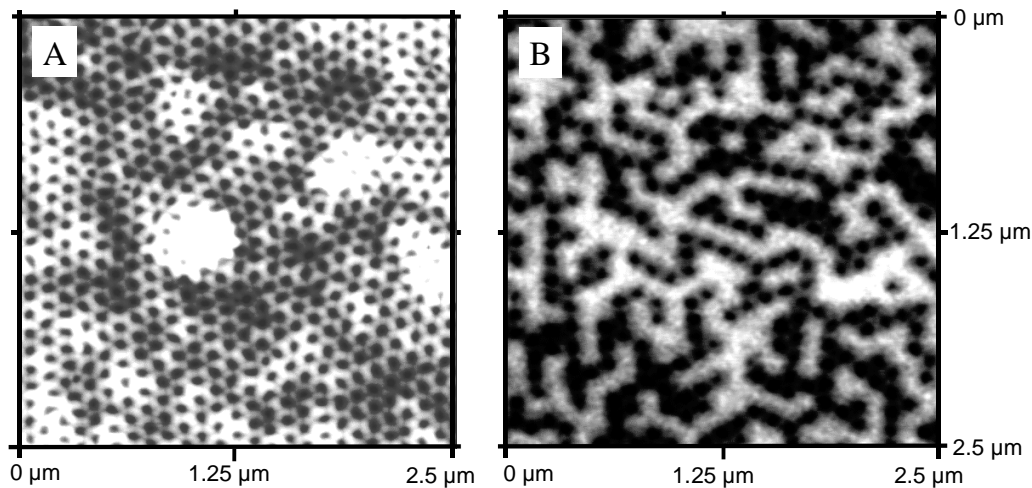


Figure 5: Topographic image of a highly-ordered porous alumina template with a pitch of 100 nm filled with $D_p \approx 35$ nm Nickel nanowires (A). The corresponding MFM image (B) of the nanomagnet array in the demagnetized state, showing the pillars magnetized alternately “up” (white) and “down” (black).

Magnetic Force Microscope (MFM) investigations show the magnetic polarization at the top of each magnetic nanowire. For example, Fig. 5(B) demonstrates the domain structure of sample (B) in the demagnetized state. Fig. 5(A) shows the corresponding topographic image. It can be deduced from the MFM data that the Ni columns are single domain nanomagnets aligned perpendicular to the surface. The patterned domain structure is due to a ferromagnetic alignment of the pillars influenced by their weak magnetic interaction. The labyrinth pattern (Fig 5(B)) of the domain structure is typical for hexagonally arranged single-domain magnetic particles with a perpendicular magnetic orientation in the demagnetized state. In Fig 5B, dark spots in the magnetic image imply a magnetization pointing up and light spots imply magnetization pointing down. Up magnetization may be interpreted as a binary ‘1’ and down magnetization as a binary ‘0’. For a perpendicular storage media, Nickel and permalloy ($\text{Ni}_{65}\text{Fe}_{35}$) seem to be suitable magnetic filling materials for porous alumina templates. Here, we have used structures with areal densities of about 75 Gbit/in² but structures with a pitch of 65 nm can boost up the areal density to 175 Gbit/in². Preliminary experiments on 65 nm-period structures show that indeed the process of Ni pulsed electrodeposition can be scaled down to smaller structure sizes.

CONCLUSION

Highly ordered porous alumina templates with a pitch of 100 nm were completely filled with Ni via pulsed electrodeposition. The bulk magnetic properties of the Ni nanowire arrays were studied by SQUID-magnetometer measurements. Reducing the diameter of the magnetic columns from $D_p = 50$ to 25 nm raises the coercivity from 600 Oe up to 1200 Oe. This is due to the reduction of the macroscopic interactions between the nanomagnets and the enhancement of the switching field of the individual nanowire. Adding an amount of Fe to the Ni-filling gives a further enhancement of the coercive field up to 1350 Oe. The domain structure of highly-ordered arrays of nickel columns is labyrinth-like as expected for anti-correlated systems on a hexagonal lattice. Each magnetic pillar is a single domain magnetic particle, magnetized perpendicular to the template surface and, in principle, can store one bit of information.

ACKNOWLEDGEMENTS

The authors would like to thank Mrs. S. Hopfe for preparing the SEM and MFM samples. We would also like to express our appreciation to Mr. T. Schweinböck and Prof. D. Weiss, University of Regensburg for discussion on the MFM data and Dr. R. Hertel, MPI for Microstructure Physics for fruitful discussions concerning magnetic modeling.

REFERENCES

1. D. Weller and A. Moser, *IEEE Trans. Magn.*, **35**, 4423 (1999).
2. R. O'Barr, S.Y. Yamamoto, S. Schultz, W. Xu, and A. Scherer, *J. Appl. Phys.*, **81**, 4730 (1997).
3. C.A. Ross, H.I. Smith, T.A. Savas, M. Schattenberg, M. Farhoud, M. Hwang, M. Walsh, M.C. Abraham, and R.J. Ram, *J. Vac. Sci. Technol.*, **B 17**, 3159 (1999).
4. M. Hwang, M.C. Abraham, T.A. Savas, H.I. Smith, R.J. Ram, and C.A. Ross, *J. Appl. Phys.*, **87**, 5108 (2000).
5. J. Raabe, R. Pulwey, R. Sattler, T. Schweinböck, J. Zweck, and D. Weiss, *J. Appl. Phys.*, **88**, 4437 (2000).
6. K. Nielsch, F. Müller, A.P. Li, and U. Gösele, *Adv. Mater.*, **12**, 582 (2000).
7. A.P. Li, F. Müller, and U. Gösele, *Electrochem. Soc. Lett.*, **3**, 131 (2000).
8. H. Masuda, H. Yamada, M. Satoh, H. Asoh, M. Nakao, and T. Tamamura, *Appl. Phys. Lett.* **71**, 2770 (1997).
9. H. Masuda and K. Fukuda, *Science*, **268**, 1466 (1995).
10. A.P. Li, F. Müller, A. Birner, K. Nielsch, and U. Gösele, *J. Appl. Phys.*, **84**, 6023 (1998).
11. R.B. Wehrspohn, A.P. Li, K. Nielsch, F. Müller, W. Erfurth and U. Gösele, *The Electrochemical Society Proceedings Series*, **PV 2000-4**, Pennington, NJ (2000), 271.
12. K. Nielsch, R.B. Wehrspohn, J. Barthel, J. Kirschner, U. Gösele, S. F. Fischer, and H. Kronmüller, *submitted to Appl. Phys. Lett.*
13. R. Hertel, unpublished results
14. K. Ounadjela, R. Ferré, L. Louail, J. M. George, and J.L. Maurice, L. Piraux, S. Dubois, *J. Appl. Phys.*, **81**, 5455 (1997).
15. M. Zheng, L. Menon, H. Zeng, Y. Liu, S. Bandyopadhyay, R.D. Kirby, and D.J. Sellmyer, *Phys. Rev. B*, **62**, 12282 (2000).
16. G.J. Strijkers, J.H.J. Dalderop, M.A.A. Broeksteeg, H.J.M. Swagten, and W.J.M. de Jonge, *J. Appl. Phys.*, **86**, 5141 (1999).